Unit 6

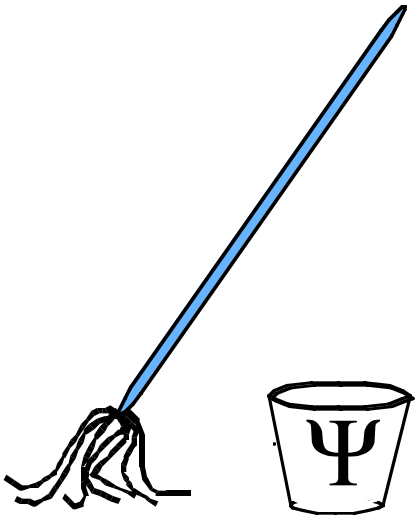

QM for AMOP

Chapter 19

Time-Variable Perturbation Of Two-State Systems

W. G. Harter

CHAPTER 19 TIME-VARIABLE PERTURBATION OF TWO-STATE SYSTEMS..... 1

For two-state systems the perturbation effects due to oscillating components A, B, C, and D of its Hamiltonian may be described analytically and geometrically. We comparison of these results with the first-order approximation given in the preceding Chapter 18. One type of the effects, as applied to transitions of NH_3 states introduced in Chapter 10, are called the AC-Stark shifts. Related effects were studied much earlier in nuclear magnetic resonance (NMR) and electronic spin resonance (ESR) systems. The effects in this Chapter are known mostly by the names Rabi-Ramsey-Schwinger and Feynman-Vernon-Helwarth after two famous papers by these triplets of authors. Rotation operator and spin vector visualization tools developed in Chapter 10 help to clarify spin resonance and time-dependent “dressed” eigenstates.

Chapter 19 Time-Variable Perturbation of Two-State Systems

19.1 "Exact" Time Dependent Perturbation

Low order approximations of time-dependent perturbation (TDP) theory is successful beyond what one has a right to expect. Using the first-order iterate (18.2.5) one may derive much of the basic theory that is used in modern physics. The constant transition rate is such a well-established result that it is called the "golden rule." Roughly speaking, TDP gives time behavior as a power series in time and the "golden rule" is based on the first term. (But, a quasi-continuum of beats has to average to zero!)

The problem with power series is that eventually they blow up. The spectral intensity function described around Fig. 18.2.1 is such an example in which $c_j^{(1)}(t)$ diverges with time t and probability $|c_j^{(1)}(t)|^2$ blows up as t^2. One should note some similarity in error growth for $c_j^{(n)}(t)$ iteration and a related failure of matrix perturbation depicted in Fig. 3.2.2 of Chapter 3.

It seems that polynomials are bad descriptors of quantum phenomena which, being fundamentally wave-like, are better described by sine, cosine, and exponential, that is, by circular and hyperbolic functions. Polynomial approximation of the two-level hyperbola in Fig. 3.2.2 eventually fails badly.

Here we consider time-dependent perturbation of a two-level system that, like the matrix perturbation example in Fig. 3.2.2, has an "exact" hyperbolic description. A hyperbolic "avoided crossing" was described again in Chapter 10 around Fig. 10.3.1 in connection with E-field splitting of ammonia (NH_3) inversion levels. This is known as a *DC Stark effect*.

This section will be devoted to basically the same problem, but with an oscillatory or AC electric field. This is known as an *AC Stark effect*. Here, as in the DC case, it will be seen how an "exact" theory can be constructed to replace a failing perturbation sequence. Such a replacement is absolutely necessary in the presence of strong coherent radiation fields of high spectral purity. Then strong quantum beats dominate and the "golden rule" goes out the window.

Among the first work to describe and demonstrate oscillatory perturbation of two-state systems was a paper by Rabi, Ramsey, and Schwinger in connection with nuclear magnetic resonance (NMR). The analogy between spin resonance and resonance of other two-state systems including NH_3-inversion was pointed out in a paper shortly thereafter by Feynman, Vernon, and Helwarth.

The NH_3-inversion experiments by Townes' group was labeled by the acronym MASER (Microwave Amplification by Stimulated Emission of Radiation). Soon thereafter, the optical transitions were found to give light amplification by stimulated emission and the LASER was born. The AC Stark effect and NMR is closely related to much of laser physics and deserves special attention not only for its historic significance but also for its fundamental quantum theoretical implications.

These implications include resonance effects in other much older 2-state systems such as optical polarization and galloping wave dynamics introduced in Chapter 4. It is ironic that earliest physical realizations of *U(2)* phenomena are the latest to receive modern attention. So-called *photonics* is both an ancient and an ultra-modern field!

(a) Perturbed 2-state systems

The most general 2-state Hamiltonian $H=H^\dagger$ has four real parameters A, B, C, and D.

$$H=\begin{pmatrix} A & B-iC \\ B+iC & D \end{pmatrix} \tag{19.1.1}$$

Chapter 10 discusses three main symmetry types of $ABCD$-Hamiltonians. First, the *AD-type* is *asymmetric-diagonal*, the *B-type* has *balanced-bilateral* symmetry, and the *C-type* is *complex-chiral* and associated with *circular* polarization, *cyclotron* resonance, or *coriolis* forces.

$$H^A=\begin{pmatrix} A & 0 \\ 0 & -A \end{pmatrix} \tag{19.1.2a}$$
$$=A\sigma_A=A\sigma_Z$$

$$H^B=\begin{pmatrix} 0 & B \\ B & 0 \end{pmatrix} \tag{19.1.2b}$$
$$=B\sigma_B=B\sigma_X$$

$$H^C=\begin{pmatrix} 0 & -iC \\ iC & 0 \end{pmatrix} \tag{19.1.2c}$$
$$=C\sigma_C=C\sigma_Y$$

(Standard XYZ labels of Pauli operators are included, too.) The general Hamiltonian (19.1.1) combines the A, B, and C symmetry operators with the $U(2)$-symmetric unit matrix operator $\sigma_0=\mathbf{1}$.

$$\mathbf{H}=\frac{A+D}{2}\mathbf{1}+\frac{A-D}{2}\sigma_A+B\sigma_B+C\sigma_C \tag{19.1.3a}$$
$$=(A+D)\mathbf{S}_0+(A-D)\mathbf{S}_A+(2B)\mathbf{S}_B+(2C)\mathbf{S}_C=\Omega_0 S_0+\Omega\bullet\mathbf{S}$$

Here the spin-$^1/_2$ angular momentum operators $\mathbf{S}_N=\sigma_N/2$ are preferred bases because their coefficients

$$\Omega_0=(A+D),\quad \Omega_A=(A-D),\quad \Omega_B=2B,\quad \Omega_C=2C. \tag{19.1.3b}$$

are angular velocities. The "crank-vector" $\mathbf{\Omega}=(\Omega_A,\Omega_B,\Omega_C)$ determines where and how fast the spin expectation value $\langle\mathbf{S}\rangle$ precesses (or if it precesses) in (S_A, S_B, S_C)-space due to an $ABCD$-Hamiltonian H.

The time Schrodinger equation, in units with $\hbar=1$, is as follows.

$$i\hbar\frac{\partial}{\partial t}\begin{pmatrix}\Psi_1\\ \Psi_2\end{pmatrix}=i\frac{\partial}{\partial t}|\Psi(t)\rangle=\mathbf{H}|\Psi(t)\rangle=\begin{pmatrix} A & B-iC \\ B+iC & D\end{pmatrix}\begin{pmatrix}\Psi_1\\ \Psi_2\end{pmatrix} \tag{19.1.4a}$$

The solution for constant A, B, C, and D is by (2.10.20) a t-exponential Ω_0-phase-plus-$\mathbf{\Omega}$-rotation.

$$|\Psi(t)\rangle=e^{-i\mathbf{H}t}|\Psi(0)\rangle=e^{-i\left(\frac{\Omega_0}{2}\mathbf{1}+\mathbf{\Omega}\bullet\mathbf{S}\right)t}|\Psi(0)\rangle=e^{-i\left(\frac{\Omega_0}{2}\mathbf{1}+\frac{\mathbf{\Omega}\bullet\mathbf{\sigma}}{2}\right)t}|\Psi(0)\rangle \tag{19.1.4b}$$
$$=e^{-i\frac{\Omega_0}{2}t}e^{-i(\Omega_A\mathbf{S_A}+\Omega_B\mathbf{S_B}+\Omega_C\mathbf{S_C})t}|\Psi(0)\rangle=e^{-i\frac{\Omega_0}{2}t}e^{-\frac{i}{2}(\Omega_A\sigma_\mathbf{A}+\Omega_B\sigma_\mathbf{B}+\Omega_C\sigma_\mathbf{C})t}|\Psi(0)\rangle$$

A similar NMR Hamiltonian for a spin moment $\mathbf{m}=g\,\mathbf{S}$ in a $\mathbf{B}$-field (but without an overall phase Ω_0) is

$$\mathbf{H}=\begin{pmatrix}\langle\uparrow|\mathbf{H}|\uparrow\rangle & \langle\uparrow|\mathbf{H}|\downarrow\rangle\\ \langle\downarrow|\mathbf{H}|\uparrow\rangle & \langle\downarrow|\mathbf{H}|\downarrow\rangle\end{pmatrix}=-\mathbf{m}\bullet\mathbf{B}=-g\mathbf{B}\bullet\mathbf{S}=\frac{g}{2}\begin{pmatrix}B_Z & B_X-iB_Y\\ B_X+iB_Y & -B_Z\end{pmatrix} \tag{19.1.5a}$$

(Again, let $\hbar=1$.) The constant-$\mathbf{B}$ solution is just an $(\mathbf{S}=\mathbf{\sigma}/2)$-vector rotation at a beat frequency Ω.

$$|\Psi(t)\rangle=e^{-ig\mathbf{B}\bullet\mathbf{S}t}|\Psi(0)\rangle=e^{-i\frac{g\mathbf{B}\bullet\mathbf{\sigma}}{2}t}|\Psi(0)\rangle=\left(\mathbf{1}\cos\frac{g|\mathbf{B}|}{2}\mathrm{t}-i\frac{\mathbf{B}\bullet\mathbf{\sigma}}{|\mathbf{B}|}\sin\frac{g|\mathbf{B}|}{2}\mathrm{t}\right), \tag{19.1.5b}$$

The *NMR beat frequency* $\Omega=g|\mathbf{B}|\hbar$ is the length of "crank vector" $\mathbf{\Omega}=g(B_X, B_Y, B_Z)$.

$$\Omega = g|\mathbf{B}| = g\sqrt{B_X^2 + B_Y^2 + B_Z^2} \qquad (19.1.5c)$$

This NMR example is essentially the same as the general *ABCD*-case except it zeros overall phase Ω_0.

Solution $|\Psi(t)\rangle$ needs to be upgraded if the parameters $\{A, B, C, D\}$ or fields (B_X,B_Y,B_Z) are time dependent. An NMR device fixes a large B_Z field to get a microwave level splitting $\Omega=gB_Z$, and oscillates low-amplitude transverse "tickler" components $B_X(t)$ or $B_Y(t)$ close to the resonance frequency Ω.

Analogous resonant transitions are stimulated in NH_3 by an E_z-field oscillating near the resonance frequency $\Omega=2S\sim24\ GHz$ of an ammonia inversion as described in Chapter 10. The Hamiltonian matrix

$$\begin{pmatrix} \langle N_{up}|\mathbf{H}|N_{up}\rangle & \langle N_{up}|\mathbf{H}|N_{dn}\rangle \\ \langle N_{dn}|\mathbf{H}|N_{up}\rangle & \langle N_{dn}|\mathbf{H}|N_{dn}\rangle \end{pmatrix} = \begin{pmatrix} H - pE_z & -S \\ -S & H + pE_z \end{pmatrix} \qquad (19.1.6a)$$

from (10.3.3) contains on its diagonal the field potential energy $-pE_z$ of an "up" Nitrogen atom state $|N_{up}\rangle$ versus $+pE_z$ of a "down" Nitrogen atom state $|N_{dn}\rangle$. Inversion tunneling amplitude $-S$ is off-diagonal. The matrix has the form of an *AB*-type Hamiltonian. Transforming to a $\{|+\rangle,|-\rangle\}$ basis interchanges S and pE_z.

$$\begin{pmatrix} \langle(+)|\mathbf{H}|(+)\rangle & \langle(+)|\mathbf{H}|(-)\rangle \\ \langle(-)|\mathbf{H}|(+)\rangle & \langle(-)|\mathbf{H}|(-)\rangle \end{pmatrix} = \begin{pmatrix} H - S & -pE_z \\ -pE_z & H + S \end{pmatrix} \text{ where: } \begin{matrix} |(+)\rangle = \left(|N_{up}\rangle + |N_{dn}\rangle\right)/\sqrt{2} \\ |(-)\rangle = \left(|N_{up}\rangle - |N_{dn}\rangle\right)/\sqrt{2} \end{matrix} \qquad (19.1.6b)$$

In an NH_3 resonance experiment, the dipole perturbation $pE_z(t)$ will be a time-dependent and is precisely analogous to the $B_X(t)$-component of the NMR "tickler" field, while NH_3 eigenstates $\{|(+)\rangle,|(-)\rangle\}$ are precisely analogous to NMR *spin-up-z* and *spin-dn-z* eigenstates $\{|\uparrow\rangle,|\downarrow\rangle\}$ in the fixed polarizing B_Z-field.

(b) Visualizing quasi-spin space: NH_3 *vs.* NMR

Generally, the *A*-axis *a.k.a. Z*-axis is the quantization axis of choice. For the NMR problem a favored-*Z* convention is forced by a big fixed B_Z-field. (A small $B_X(t)$ will be wiggled.) For the NH_3 problem we plan to wiggle $B=-pE_z(t)$ in (19.1.6b) and not S. (Nature fixes tunneling amplitude S.) *NH_3* eigenstates $\{|(+)\rangle,|(-)\rangle\}$ will now be associated with *spin-up-A* and *spin-down-A*, with field-free eigenvalues $A=H-S$ and $D=H+S$, respectively. In going between (19.1.6a and b), A and B are switched.

Do not confuse the *z*-axis of the NH_3 molecule with the *A* or *Z*-axis in its quasi-spin (S_A, S_B, S_C)-space. Nor is the *x*-axis of the NH_3 molecule to be confused with the *B* or *X*-axis. But, all three **B**-field components $(B_X(t),B_Y(t),B_Z)$ are meaningful real parameters $\{A=B_Z, B=B_X(t), C=B_Y(t), D=-B_Z,\}$ of the NMR Hamiltonian (19.1.5a), while the NH_3 inversion Hamiltonian (19.1.6b) has only the *z*-dipole energy $pE_z(t)$ as a meaningful real field parameter in the set $\{A=H-S, B=-pE_z(t), C=0, D=H+S\}$.

The dipole *balance parameter B* quantifies a $(-q\mathbf{E}\bullet\mathbf{r})$ coupling between two states $|(+)\rangle$ and $|(-)\rangle$.

$$B=-pE_z(t)=-\langle(+)|q\mathsf{z}E_z(t)|(-)\rangle = r\cos(\omega t)=(r/2)(e^{i\omega t}+e^{-i\omega t}) \qquad (19.1.7a)$$

B is $gB_x(t)/2$ for the NMR example. For NH_3 it is the *interaction strength* or *Rabi rate parameter r*.

$$B= r = -pE_z(0) \qquad (19.1.7b)$$

B contains the oscillator strength or *electric dipole matrix element*

$$p=q\langle(+)|\mathsf{z}|(-)\rangle, \qquad (19.1.7c)$$

in product with the field magnitude $E_z(0)$ for which a real monochromatic radiation field is assumed.

$$E_z(t) = \cos(\omega t)=(1/2)(e^{i\omega t}+e^{-i\omega t}) \ . \qquad (19.1.7d)$$

Below is the exact NH_3 inversion-resonance Hamiltonian (19.1.6b) in its Schrodinger equation.

$$i\frac{\partial}{\partial t}\begin{pmatrix}\psi_+\\ \psi_-\end{pmatrix}=\begin{pmatrix}H+\frac{\varepsilon}{2} & \frac{r}{2}\cos\omega t\\ \frac{r}{2}\cos\omega t & H-\frac{\varepsilon}{2}\end{pmatrix}\begin{pmatrix}\psi_+\\ \psi_-\end{pmatrix}, \quad \text{where: } \varepsilon=-2S \qquad (19.1.8a)$$

The **H**-crank **Ω**-components (19.1.3b) are below. The unperturbed *(r=0)* case is shown in Fig. 19.1.1b.

$$\Omega_0 = H\ , \qquad \Omega_A = \varepsilon, \quad \Omega_B = r\cos\omega t, \quad \Omega_C = 0. \qquad (19.1.8b)$$

The **H**-crank vector **Ω** swings to-and-fro in the AB-plane at constant $\Omega_A=\varepsilon$ as shown later. (Fig. 19.1.2b)

The NH_3-electric dipole moment of any state is related to the transverse $\langle\mathbf{S}_\perp\rangle$–component of the quasi-spin vector $\langle\mathbf{S}\rangle$ expectation. In NMR, $\langle\mathbf{m}_\perp\rangle=g\langle\mathbf{S}_\perp\rangle$ is the magnetic moment transverse to the main B_Z-field. The NH_3 dipole $\langle p_z\rangle=q\langle z\rangle$ is a product of p and $2S_B=2\mathrm{Re}\psi_+^*\psi_-$ using (2.10.8b) and (19.1.7).

$$\begin{aligned}\langle p_z\rangle &= \langle\Psi|\rho_z|\Psi\rangle = \left(\psi_+^*\langle+|+\psi_-^*\langle-|\right)\rho_z\left(\psi_+|+\rangle+\psi_-|-\rangle\right)\\ &= 2\mathrm{Re}\psi_+^*\psi_-\langle+|\rho_z|-\rangle \quad (\text{using } \langle+|\rho_z|-\rangle=\langle-|\rho_z|+\rangle) \qquad (19.1.9a)\\ &= 2S_B p = p\cos\alpha\sin\beta \quad (\text{using (2.10.8b) and } \langle+|\rho_z|-\rangle = p)\end{aligned}$$

Symmetry rules out diagonal z-matrix elements $\langle+|z|+\rangle=0=\langle-|z|-\rangle$. Here is the time derivative of $\langle p_z\rangle$.

$$\begin{aligned}\langle\dot\rho_z\rangle &= \langle\dot\Psi|\rho_z|\Psi\rangle+\langle\Psi|\rho_z|\dot\Psi\rangle = \left(\dot\psi_+^*\psi_-+\dot\psi_-^*\psi_++\psi_+^*\dot\psi_-+\psi_-^*\dot\psi_+\right)\langle+|\rho_z|-\rangle\\ &= -2\varepsilon\,\mathrm{Im}\psi_+^*\psi_-\langle+|\rho_z|-\rangle \qquad (\text{using: } i\dot\psi_\pm=\pm\frac{\varepsilon}{2}\psi_\pm\ ) \qquad (19.1.9b)\\ &= -2\varepsilon S_C p = -\varepsilon p\sin\alpha\sin\beta \qquad (\text{using (2.10.8b) and } \langle+|\rho_z|-\rangle = p)\end{aligned}$$

Fig. 19.1.1a shows a "real" NMR spin moment $\mathbf{m}=g\mathbf{S}$ precessing around its Ω-cranking gB_Z-field. Fig. 19.1.1b shows an analogous NH_3 quasi-spin **S** similarly precessing around its A-axis at rate $\varepsilon=2S$. The transverse NMR moment $\mathbf{m}_\perp$ lies in the projection or "shadow" of **m** in the XY-plane. An analogous NH_3 *Lorentz phasor* vector $\mathbf{p}_\perp=q(\langle z\rangle,-\langle\dot z\rangle/\varepsilon)$ rotates in the BC-plane according to (19.1.9) at rate $\Omega=2S=\varepsilon$. This relates the first Euler angle α to an *atomic oscillator phase angle* $\phi=-\alpha$, as shown in Fig. 19.1.1b.

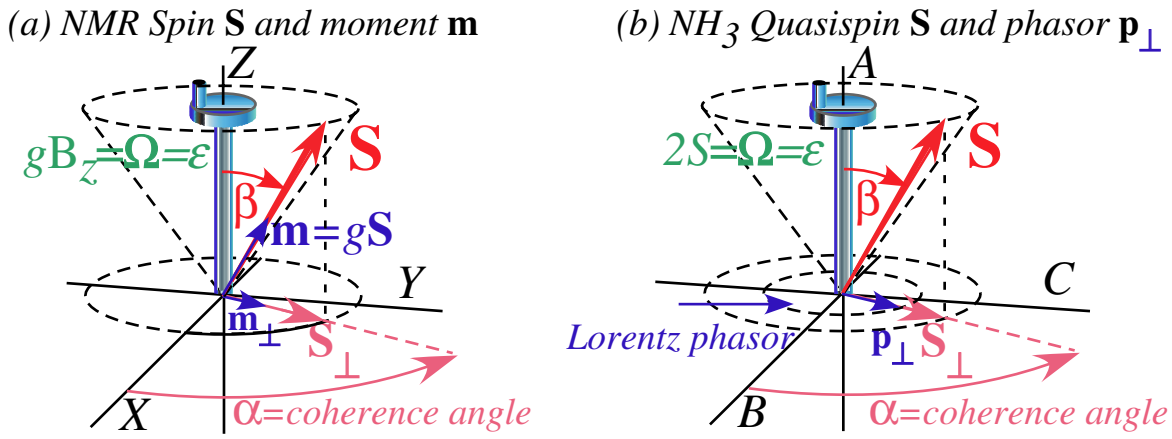

Fig. 19.1.1 Ω-Cranked polarization and spin vectors for (a) NMR and (b) NH_3 inversion resonance.

$\mathbf{p}_\perp$ is a quantum version of the classical Lorentz atomic oscillator phasor $p(t)=p(0)e^{-i\varepsilon t}$ which has a real value $p(0)\cos\varepsilon t$ and an imaginary value $-p(0)\sin\varepsilon t$ corresponding to dipole time derivative $(dp/dt)/\varepsilon$.

Lorentz oscillators are classical harmonic oscillators and grow to infinity if the driving frequency ω approaches the natural frequency $\Omega=\varepsilon$. Not so for the quantum model of a two level atom pictured in Fig. 19.1.1b. The dipole expectation value $\langle p_z\rangle=q\langle z\rangle$ starts at zero for the ground $|(+)\rangle$-eigenstate $(\beta=0)$ then grows toward its *saturation* value of p for a (50-50) state such as a *spin-up-B* wave $(\psi_+,\psi_-)=(1/\sqrt{2},\ 1/\sqrt{2})$ with spin at $\beta=\pi/2$. The value p is as large as $\langle p_z\rangle$ can be for the 2-level system.

Saturated (50-50)-states have **S**-vector normal $(\beta=\pi/2)$ to the crank **Ω**-vector. This includes the Nitrogen-up state $|N_{up}\rangle=(|(+)\rangle+|(-)\rangle)/\sqrt{2}$ the Nitrogen-down state $|N_{dn}\rangle=(|(+)\rangle-|(-)\rangle)/\sqrt{2}$ whose **S**-vector is along the $\pm B$-axes, or transition states $|\pm C\rangle=(|(+)\rangle\pm i|(-)\rangle)/\sqrt{2}$ whose **S**-vector is along the $\pm C$-axes. An increase in amount of excited state $|(-)\rangle$ above 50-50 *decreases* the dipole moment in the BC-plane; it is zero for a pure excited state $|(-)\rangle$ or a pure ground state $|(+)\rangle$. Lorentz "phasor space" unbounded and flat, but a 2-state $(|(+)\rangle,|(-)\rangle)$ phasor or *coherence* space is a bounded spherical projection and periodic. The quantum quasi-spin world, unlike Lorentz's "flat" classical phasor world, is "round."

(c) Rotating wave solutions

We first solve a *rotating wave approximation* to (19.1.8) obtained by dropping $e^{i\omega t}$ from $E_z(t)$.

$$i\frac{\partial}{\partial t}\begin{pmatrix}\psi_1\\ \psi_2\end{pmatrix}=\begin{pmatrix}\frac{\varepsilon}{2} & \frac{r}{2}e^{-i\omega t}\\ \frac{r}{2}e^{+i\omega t} & \frac{-\varepsilon}{2}\end{pmatrix}\begin{pmatrix}\psi_1\\ \psi_2\end{pmatrix},\ \text{where: } \varepsilon=-2S\ ,\ \text{and: } \begin{matrix}\psi_1=\psi_+=\psi_\uparrow\\ \psi_2=\psi_-=\psi_\downarrow\end{matrix} \qquad (19.1.10a)$$

The **H**-crank vector **Ω** rotates around the Z-axis tracing an inverted cone of altitude ε as in Fig. 19.1.2a.

$$\Omega_0=H=0,\quad \Omega_Z=\Omega_A=\varepsilon,\ \Omega_X=\Omega_B=r\cos\omega t,\ \Omega_Y=\Omega_C=r\sin\omega t. \qquad (19.1.10b)$$

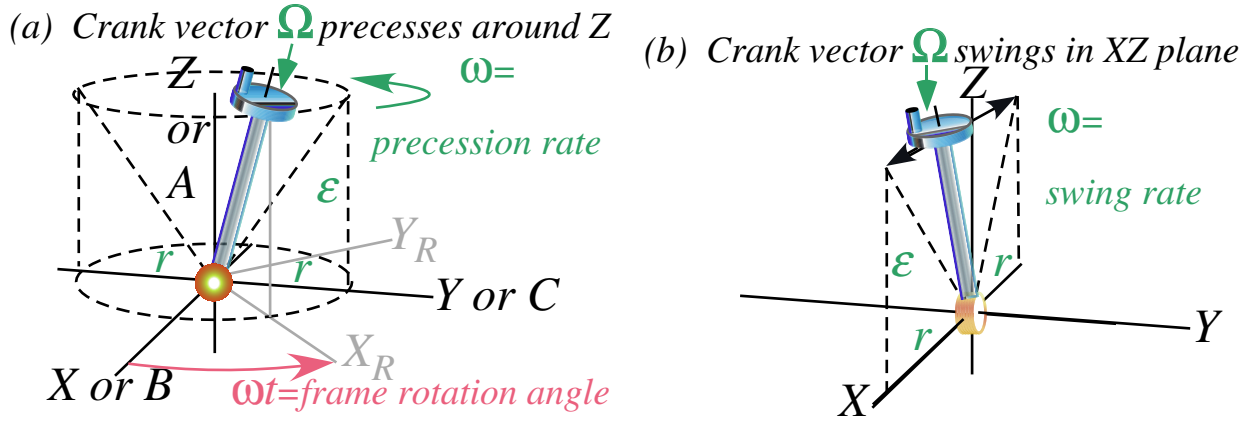

Fig. 19.1.2 Ω-Crank time dependence for (a) Rotating crank approximation (b) Exact planar swing.

This **H** is like that of an NMR resonance with a fixed B_z field added to a rotating $B_x(t)$ and $B_y(t)$ field.

$$B_z = 2\varepsilon, \quad B_x(t) = 2r\cos\omega t, \quad B_y(t) = 2r\sin\omega t. \tag{19.1.10c}$$

For such a **B**-field (19.1.10a) is an exact equation. In the analogous NH_3 equation (19.1.8) only the *X*-or-*B*-component oscillates as shown in Fig. 19.1.2b. But, it turns out that the circular polarized **B** or **Ω** motion (19.1.10b-c) like Fig. 19.1.2a has much the same effect as a *ZX*-plane swinging **Ω** (19.1.8b) in Fig. 19.1.2b provided the amplitude B_x (or Rabi radius *r*) is much less than the splitting frequency ε ($r<<\varepsilon$).

To solve (19.1.10a) we boost by rotation $R_Z[\omega t]$ to a rotating frame $\{X_R, Y_R, Z_R, =Z\}$ shown in Fig. 19.1.2a, where the crank vector **Ω** would appear to be standing still. This is something like the change-of-picture boost which zeros the vector potential **A** in (17.1.16). New *R*-base states $|k\rangle^R$ are defined first.

$$|\uparrow\rangle^R = \mathsf{R}_Z[\omega t]|\uparrow\rangle = e^{-i\omega t\,J_Z}|\uparrow\rangle = e^{-i\omega t/2}|\uparrow\rangle, \quad {}^R\langle\uparrow| = \langle\uparrow|\mathsf{R}^\dagger[\omega t] = \langle\uparrow|e^{+i\omega t/2} \tag{19.1.11a}$$

$$|\downarrow\rangle^R = \mathsf{R}_Z[\omega t]|\downarrow\rangle = e^{-i\omega t\,J_Z}|\downarrow\rangle = e^{+i\omega t/2}|\downarrow\rangle, \quad {}^R\langle\downarrow| = \langle\downarrow|\mathsf{R}^\dagger[\omega t] = \langle\downarrow|e^{-i\omega t/2} \tag{19.1.11b}$$

This gives the needed transformation matrix and inverse.

$$\begin{pmatrix} \langle\uparrow|\uparrow\rangle^R & \langle\uparrow|\downarrow\rangle^R \\ \langle\downarrow|\uparrow\rangle^R & \langle\downarrow|\downarrow\rangle^R \end{pmatrix} = \begin{pmatrix} e^{-i\omega t/2} & 0 \\ 0 & e^{+i\omega t/2} \end{pmatrix} \qquad \begin{pmatrix} {}^R\langle\uparrow|\uparrow\rangle & {}^R\langle\uparrow|\downarrow\rangle \\ {}^R\langle\downarrow|\uparrow\rangle & {}^R\langle\downarrow|\downarrow\rangle \end{pmatrix} = \begin{pmatrix} e^{+i\omega t/2} & 0 \\ 0 & e^{-i\omega t/2} \end{pmatrix} \tag{19.1.11c}$$

Then transformed wave amplitudes $\psi^R = \mathsf{R}^\dagger\psi$ and a new Hamiltonian $\mathsf{H}^R = \mathsf{R}^\dagger\mathsf{H}\cdot\mathsf{R}$ follow.

$$\begin{pmatrix} \psi^R_\uparrow \\ \psi^R_\uparrow \end{pmatrix} = \begin{pmatrix} {}^R\langle\uparrow|\psi\rangle \\ {}^R\langle\downarrow|\psi\rangle \end{pmatrix} = \begin{pmatrix} {}^R\langle\uparrow|\uparrow\rangle & {}^R\langle\uparrow|\downarrow\rangle \\ {}^R\langle\downarrow|\uparrow\rangle & {}^R\langle\downarrow|\downarrow\rangle \end{pmatrix}\begin{pmatrix} \langle\uparrow|\psi\rangle \\ \langle\downarrow|\psi\rangle \end{pmatrix} = \begin{pmatrix} e^{+i\omega t/2} & 0 \\ 0 & e^{-i\omega t/2} \end{pmatrix}\begin{pmatrix} \psi_\uparrow \\ \psi_\downarrow \end{pmatrix} \tag{19.1.11d}$$

The new Hamiltonian H^R does indeed have a constant **Ω**-vector and no explicit time dependence.

$$\begin{pmatrix} {}^R\langle\uparrow|H|\uparrow\rangle^R & {}^R\langle\uparrow|H|\downarrow\rangle^R \\ {}^R\langle\downarrow|H|\uparrow\rangle^R & {}^R\langle\downarrow|H|\downarrow\rangle^R \end{pmatrix} = \begin{pmatrix} {}^R\langle\uparrow|\uparrow\rangle & {}^R\langle\uparrow|\downarrow\rangle \\ {}^R\langle\downarrow|\uparrow\rangle & {}^R\langle\downarrow|\downarrow\rangle \end{pmatrix}\begin{pmatrix} \langle\uparrow|H|\uparrow\rangle & \langle\uparrow|H|\downarrow\rangle \\ \langle\downarrow|H|\uparrow\rangle & \langle\downarrow|H|\downarrow\rangle \end{pmatrix}\begin{pmatrix} \langle\uparrow|\uparrow\rangle^R & \langle\uparrow|\downarrow\rangle^R \\ \langle\downarrow|\uparrow\rangle^R & \langle\downarrow|\downarrow\rangle^R \end{pmatrix} \tag{19.1.12}$$

$$= \begin{pmatrix} e^{+i\omega t/2} & 0 \\ 0 & e^{-i\omega t/2} \end{pmatrix}\begin{pmatrix} \varepsilon/2 & re^{-i\omega t}/2 \\ re^{-i\omega t}/2 & -\varepsilon/2 \end{pmatrix}\begin{pmatrix} e^{-i\omega t/2} & 0 \\ 0 & e^{+i\omega t/2} \end{pmatrix} = \begin{pmatrix} \varepsilon/2 & r/2 \\ r/2 & -\varepsilon/2 \end{pmatrix}$$

But, change-of-picture (19.1.11d) has time dependence so time derivative $i\partial/\partial t\ \psi^R$ yields extra terms.

$$i\frac{\partial}{\partial t}\begin{pmatrix}\psi^R_\uparrow\\ \psi^R_\downarrow\end{pmatrix}= \quad i\frac{\partial}{\partial t}\begin{pmatrix}e^{+i\omega t/2} & 0\\ 0 & e^{-i\omega t/2}\end{pmatrix}\begin{pmatrix}\psi_\uparrow\\ \psi_\downarrow\end{pmatrix}+\begin{pmatrix}e^{+i\omega t/2} & 0\\ 0 & e^{-i\omega t/2}\end{pmatrix}i\frac{\partial}{\partial t}\begin{pmatrix}\psi_\uparrow\\ \psi_\downarrow\end{pmatrix} \tag{19.1.13a}$$

$$=\begin{pmatrix}\frac{-\omega}{2} & 0\\ 0 & \frac{\omega}{2}\end{pmatrix}\begin{pmatrix}e^{+i\omega t/2} & 0\\ 0 & e^{-i\omega t/2}\end{pmatrix}\begin{pmatrix}\psi_\uparrow\\ \psi_\downarrow\end{pmatrix}+\begin{pmatrix}e^{+i\omega t/2} & 0\\ 0 & e^{-i\omega t/2}\end{pmatrix}\mathsf{H}\begin{pmatrix}\psi_\uparrow\\ \psi_\downarrow\end{pmatrix} \tag{19.1.13b}$$

The original Schrodinger equation $i\partial/\partial t|\psi\rangle=\mathsf{H}|\psi\rangle$ becomes one for $|\psi^R\rangle=\mathsf{R}^\dagger[\omega t]|\psi^R\rangle$ by inserting $\mathsf{R}^\dagger\mathsf{R}=1$.

$$i\frac{\partial}{\partial t}\begin{pmatrix}\psi^R_\uparrow\\ \psi^R_\downarrow\end{pmatrix}=\begin{pmatrix}\frac{-\omega}{2} & 0\\ 0 & \frac{\omega}{2}\end{pmatrix}\cdot\mathsf{R}^\dagger[\omega t]\cdot\begin{pmatrix}\psi_\uparrow\\ \psi_\downarrow\end{pmatrix}+\mathsf{R}^\dagger[\omega t]\cdot\mathsf{H}\cdot\mathsf{R}[\omega t]\mathsf{R}^\dagger[\omega t]\begin{pmatrix}\psi_\uparrow\\ \psi_\downarrow\end{pmatrix} \tag{19.1.14}$$

The new H^R has extra diagonal terms $\pm\omega/2$ but off-diagonal time dependence $e^{\pm i\omega t}$ of (19.1.10) is gone.

$$i\frac{\partial}{\partial t}\left|\psi^R\right\rangle=\mathsf{R}^\dagger\mathsf{H}\mathsf{R}\left|\psi^R\right\rangle=\mathsf{H}^R\left|\psi^R\right\rangle \quad \text{or:} \quad i\frac{\partial}{\partial t}\begin{pmatrix}\psi^R_\uparrow\\ \psi^R_\downarrow\end{pmatrix}=\begin{pmatrix}\frac{\varepsilon-\omega}{2} & \frac{r}{2}\\ \frac{r}{2} & \frac{-\varepsilon+\omega}{2}\end{pmatrix}\begin{pmatrix}\psi^R_\uparrow\\ \psi^R_\downarrow\end{pmatrix} \tag{19.1.15a}$$

The crank vector $\mathbf{\Omega}^R$ in the rotating frame is indeed motionless but has $(-\omega)$ added to its Z-component.

$$\Omega^R{}_0 = H^R{}_{11}+H^R{}_{22}, \quad \Omega_Z = H^R{}_{11}-H^R{}_{22}, \quad \Omega_X = 2\mathrm{Re}H^R{}_{12}, \quad \Omega_Y = 2\mathrm{Im}H^R{}_{12}.$$
$$= 0, \qquad = \varepsilon-\omega=\Delta, \qquad = r, \qquad = 0. \tag{19.1.15b}$$

The resulting crank $\mathbf{\Omega}^R$ depends on the *detuning* parameter $\Delta=\varepsilon-\omega$ as shown in Fig. 19.1.3. Δ is zero at resonance. A zero detuning makes the beat frequency or crank length become a minimum value r.

$$\Omega^R=\pm\sqrt{\Delta^2+r^2}\cong\begin{cases}\pm\Delta & \text{for: } r<<|\Delta| \text{ (far from resonance)}\\ \pm r & \text{for: } |\Delta|<<r \text{ (close to resonance)}\end{cases} \tag{19.1.15c}$$

The minimum beat frequency r is called the *Rabi frequency* and was given (for $\hbar=1$) by (19.1.7).

$$r = -q\langle(+)|\mathsf{z}|(-)\rangle E_z(0) \tag{19.1.16}$$

Two-state quantum resonant beat frequency Ω^R, unlike a classical resonance, approaches r but not zero as detuning Δ goes through zero. But, when detuning exceeds r, we recover the classical relation $\Omega^R=\Delta$ between beat rate and natural-minus-stimulus frequency difference $\Delta=\varepsilon-\omega$, as shown in (19.1.15c).

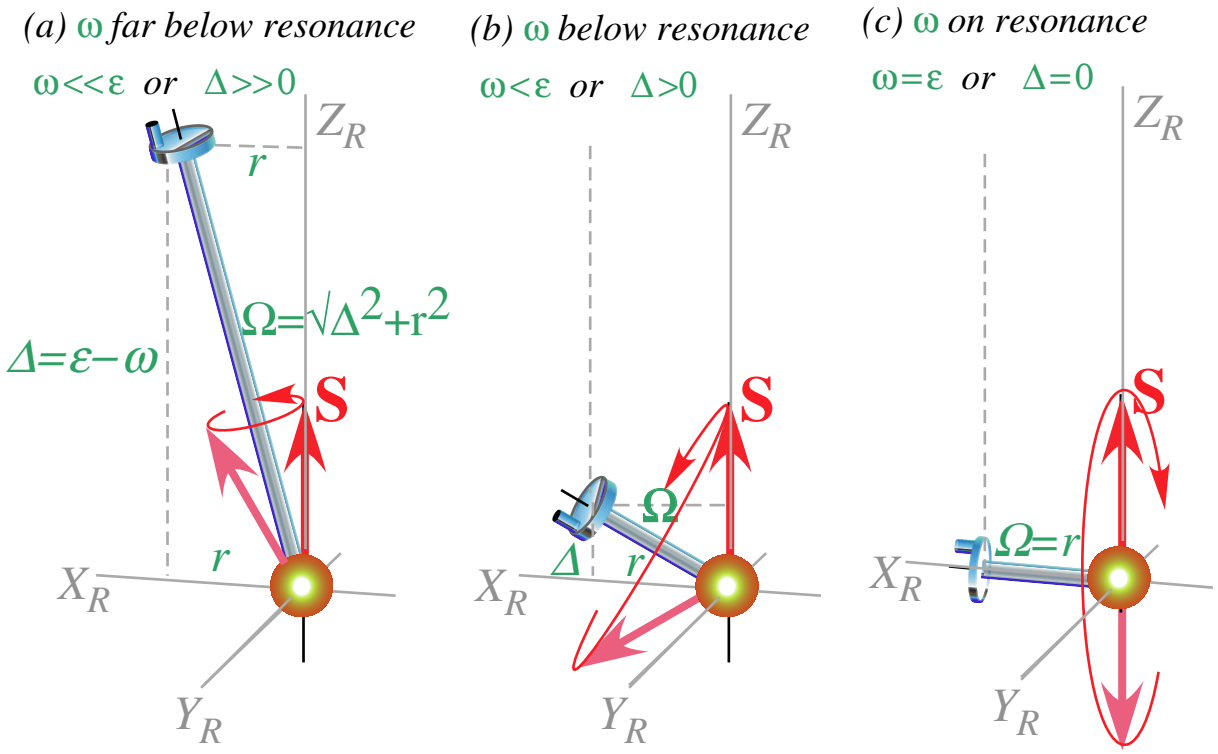

Fig. 19.1.3 $\mathbf{\Omega}^R$*-crank turns spin S-up state in rotating frame (a)* $\omega<<\varepsilon$ *(b)*$\omega<\varepsilon$ *(c) Resonance* $\omega=\varepsilon$.

Two-state quantum response does not blow up at $\Delta=0$ like the classical Lorentz oscillator (18.3.1) or like the first order approximation (18.2.6). As noted after Fig. 19.1.1, maximum dipole response has its spin **S** normal to the *Z*-axis *(*$\beta=\pi/2$*)*. This happens to an initial ground state (*spin-up* $|\uparrow\rangle^R$) if Δ lies inside $\pm r$ as in Fig. 19.1.3b-c. Time evolution operator $U^R(t)=e^{-iH^Rt}$ is a rotation around crank $\mathbf{\Omega}^R$ of polar angle ϑ^R for $\cos\vartheta^R=\Delta/\Omega^R$ and $\sin\vartheta^R=r/\Omega^R$. Rotation matrix $e^{-i\mathbf{\Omega}t\bullet\mathbf{J}}$ comes from (10.5.25c) in Ch. 10.

$$U^R(t)|\uparrow\rangle^R = e^{-i\mathbf{\Omega}^R t\bullet\mathbf{J}}|\uparrow\rangle^R = \begin{pmatrix} \cos\frac{\Omega^R t}{2} - i\cos\vartheta^R \sin\frac{\Omega^R t}{2} & \cdot \\ -i\sin\vartheta^R \sin\frac{\Omega^R t}{2} & \cdot \end{pmatrix}\begin{pmatrix}1\\0\end{pmatrix} = \begin{pmatrix} \cos\frac{\Omega^R t}{2} - i\frac{\Delta}{\Omega^R}\sin\frac{\Omega^R t}{2} & \cdot \\ -i\frac{r}{\Omega^R}\sin\frac{\Omega^R t}{2} & \cdot \end{pmatrix} \tag{19.1.17}$$

The excited $|\downarrow\rangle^R$-state component gives the transition probability from ground $|\uparrow\rangle^R$-state as a function of time *t*, Rabi amplitude *r*, and detuning Δ. For large Δ it reduces to the spectral intensity value (18.2.6).

$$\begin{aligned} \left|{}^R\langle\downarrow|\psi(t)\rangle\right|^2 &= \left(\frac{r}{\Omega^R}\sin\frac{\Omega^R t}{2}\right)^2 = \frac{r^2}{\Delta^2+r^2}\sin\frac{\sqrt{\Delta^2+r^2}\,t}{2} \\ &\cong \frac{r^2\sin^2 t\Delta/2}{\Delta^2} = \frac{r^2}{4}|S(\Delta,t)|^2 \quad \text{for: } |\Delta|>>r \end{aligned} \tag{19.1.18}$$

A plot of 2-state transition is given in Fig. 19.1.4 to compare with a first order approximation in Fig. 18.2.1. The Rabi surface in Fig. 19.1.4 below has the same markings as the first-order approximation in Fig. 18.2.1. Notice the uncertainty hyperbolas that are at the bottom of valleys in Fig. 18.2.1 have been lifted up in Fig.

19.1.4 by encroaching beatlet peaks that used to surround them. This lifting effect becomes most pronounced near the resonance origin (Δ=0) but diminishes in regions far from resonance.

As mentioned before, the first-order approximation is most happy to stay away from resonance where it unhappily blows up. Fig. 18.2.1 and Fig. 19.1.4 are practically the same everywhere except in the tiny region blown up in the two figures.

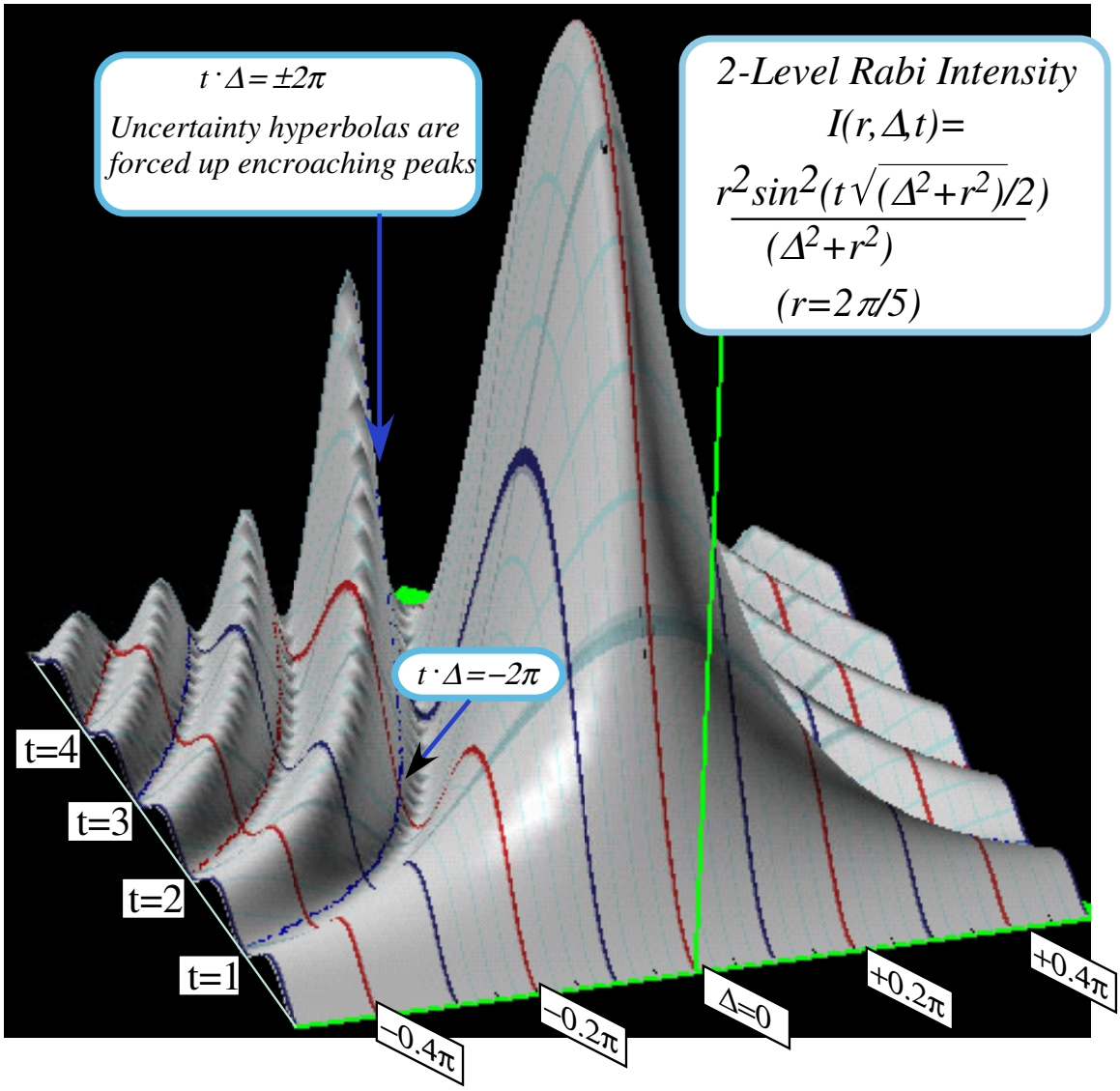

Fig. 19.1.4 Rabi spectral intensity function I(r,Δ,t) for 2-level rotating wave for r=2π/5.

The most striking contrast between Rabi 2-level *I(r,Δ,t)* and the approximate *I(Δ,t)* is that the Rabi *(Δ=0)*-peak goes to a maximum value: *I(r, Δ=0, t=π/r)=1* then back to zero at *t=2π/r. Meanwhile*, the approximate $I(\Delta=0,t)=t^2$ just goes up! In other words, after one Rabi period, the transition probability is back to zero since the spin vector in Fig. 19.1.3c has completed one full revolution. No such return to initial state is possible in a first (or even 2nd or 3rd) order polynomial perturbation approximation.

Rabi 2-level response $I(r,\Delta,t)$ beats faster than $I(\Delta,t)$ near $\Delta=0$. Beat rate Ω^R (19.1.15c) depends on stimulus amplitude through Rabi rate r as well as on stimulus frequency ω through $\Delta=\varepsilon-\omega$. If r increases, beats get faster and bigger near $\Delta=0$ since Rabi-r is both a *rate* and a *radius* of $\mathbf{\Omega}^R$-cranking. A top view of $I(r,\Delta,t)$ with twice the rate r $(r=4\pi/5)$ is shown below in Fig. 19.1.5. Note how the zeros of $I(r,\Delta,t)$ veer away from uncertainty hyperbolas of $I(r,t)$ and toward a $(\Delta=0)$-rendezvous at each Rabi period.

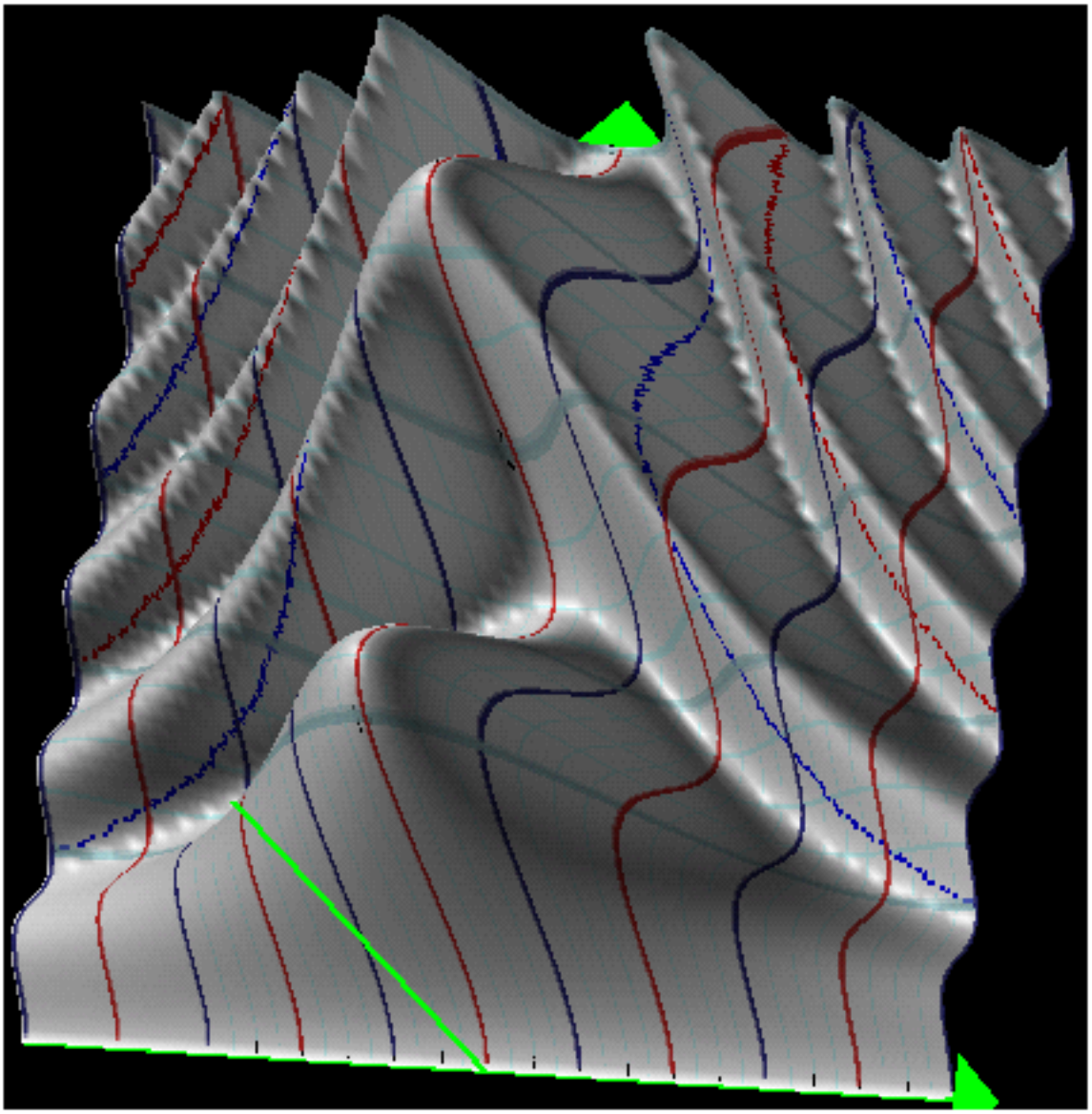

Fig. 19.1.5 Top-down view of Rabi spectral intensity function $I(r,\Delta,t)$ for $r=4\pi/5$.

As zeros move toward low-Δ, the probability moves away. Larger and faster beats also appear in the $\pm\Delta$ wings of the spectrum as r is increased. This effect, known as *power broadening*, changes the spectral profile (19.1.17) from a narrow inverse-Δ-square (r^2/Δ^2) to a fatter Lorentzian $(r^2/[\Delta^2+r^2])$.

The frame $\{X_R, Y_R, Z_R,\}$ of Fig. 19.1.3 rotates at the stimulus frequency ω about the $(Z=Z_R)$-axis as shown in Fig. 19.1.2. So, an X_R, spin component or related polarization $\mathbf{p}_\perp$ or $\mathbf{m}_\perp$in Fig. 19.1.2 also has a ω-field-driven rotation. Oscillation or rotation of electric or magnetic moments radiates electromagnetic waves at the frequency ω of the oscillation. ω-Radiation from 2-state system rises when the slower $\mathbf{\Omega}^R$-rotation drives the spin vector **S** away from the Z_R-axis in Fig. 19.1.3, but it falls as the same $\mathbf{\Omega}^R$ brings **S** back to the Z_R-axis. Neither a pure ground state $|(+)\rangle$ or $|\uparrow\rangle$ nor a pure excited state $|(-)\rangle$ or $|\downarrow\rangle$ can radiate. Radiating moments require state mixture, preferably a saturated 50-50 mixture.

(d) AC Stark levels: Dressed eigenstates

To better understand an increasingly intimate relation between atomic and nuclear moments for two levels $(E\uparrow=0,\ E\downarrow=\hbar\varepsilon)$ and its stimulating radiation field $E_R=\hbar\omega$, let us plot the important frequencies as a function of *detuning* Δ=ε−ω by the *stimulus frequency* ω off the *zero-field transition frequency* ε. The simplest of these plots is the zero-coupling case of Fig. 19.1.6a for which the Rabi-rate is zero. $(r=0)$ It is a 45° line representing the laser stimulus crossing horizontal lines representing the two levels 0 and ε.

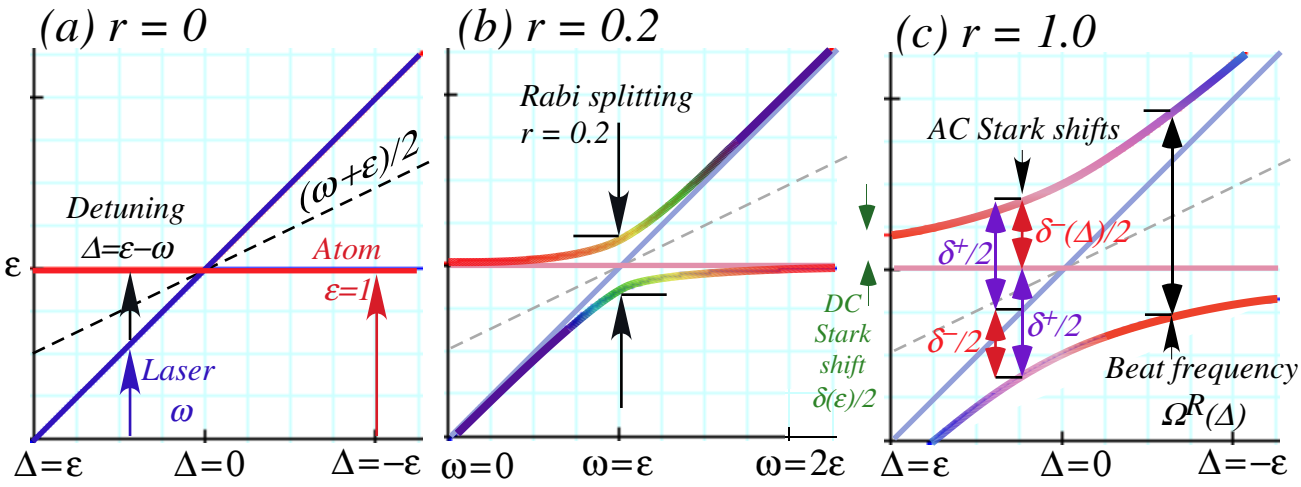

Fig. 19.1.6 Rotating wave eigenfrequencies versus detuning frequency. Rabi rate r=(a) 0, (b) 0.2, (c) 1.0.

Plotted are eigenvalues of the rotating wave Hamiltonian (19.1.15) plus an overall frequency $\Omega_0=(\varepsilon+\omega)/2$.

$$\mathsf{H}^R+\Omega_0\mathsf{1}=\begin{pmatrix}\frac{\Delta}{2} & \frac{r}{2}\\ \frac{r}{2} & \frac{-\Delta}{2}\end{pmatrix}+\Omega_0\mathsf{1}=\begin{pmatrix}\frac{\varepsilon-\omega}{2} & \frac{r}{2}\\ \frac{r}{2} & \frac{-\varepsilon+\omega}{2}\end{pmatrix}+\frac{\varepsilon+\omega}{2}\mathsf{1}=\begin{pmatrix}\varepsilon & \frac{r}{2}\\ \frac{r}{2} & \omega\end{pmatrix} \qquad (19.1.19)$$

Eigenvalues of $\mathsf{H}^R+\Omega_0\,\mathsf{1}$ are called *dressed eigenfrequencies* $\Omega_0\pm\Omega^R/2$. Ω^R is the crank rate (19.1.15c).

$$\Omega^{hi}=\Omega_0+\Omega^R/2=\varepsilon+(\Omega^R-\varepsilon+\omega)/2=\varepsilon+(\Omega^R-\Delta)/2=\varepsilon+\delta^-/2 \qquad (19.1.20a)$$

$$\Omega^{lo}=\Omega_0-\Omega^R/2=\omega-(\Omega^R-\varepsilon+\omega)/2=\omega-(\Omega^R-\Delta)/2=\omega-\delta^-/2 \qquad (19.1.20b)$$

Eigenstate $|\Omega^{hi}\rangle$ or $|\Omega^{lo}\rangle$ has spin **S** aligned or anti-aligned to crank vector $\mathbf{\Omega}^R$. ($\beta=\vartheta^R$ or $\beta=\pi+\vartheta^R$)

The polar angle ϑ^R of the rotating crank $\mathbf{\Omega}^R$ is shown in Fig. 19.1.3 with $\cos\vartheta^R=\Delta/\Omega^R$ and $\sin\vartheta^R=r/\Omega^R$.

The eigenstate components use $\cos^2\vartheta^R/2=(1+\Delta/\Omega^R]/2$ and $\sin^2\vartheta^R/2=(1-\Delta/\Omega^R]/2$ to give *AC-Stark states*

$$\left|\Omega^{lo}\right\rangle^D=\begin{pmatrix}\cos\frac{\vartheta^R}{2}\\ \sin\frac{\vartheta^R}{2}\end{pmatrix}=\begin{pmatrix}\frac{r}{\sqrt{2\Omega^R\delta^-}}\\ \frac{\delta^-}{\sqrt{2\Omega^R\delta^-}}\end{pmatrix},\quad(19.1.20c)\qquad \left|\Omega^{hi}\right\rangle^D=\begin{pmatrix}-\sin\frac{\vartheta^R}{2}\\ \cos\frac{\vartheta^R}{2}\end{pmatrix}=\begin{pmatrix}\frac{-\delta^-}{\sqrt{2\Omega^R\delta^-}}\\ \frac{r}{\sqrt{2\Omega^R\delta^-}}\end{pmatrix},\quad(19.1.20d)$$

where we define the *AC-Stark shifts* $\delta^\pm$ as follows. (See also: Fig. 19.1.6.)

$$\delta^-=\delta(\Delta)\ =\Omega^R-\Delta=\sqrt{[\Delta^2+r^2]}-\Delta \qquad (19.1.20e)$$

$$\delta^+=\delta(-\Delta)=\Omega^R+\Delta=\sqrt{[\Delta^2+r^2]}+\Delta \qquad (19.1.20e)$$

Half shifts $\delta^-/2$ and $\delta^+/2$ give the deviation of each eigenfrequency from the zero-field frequencies ω or ε as seen in (19.1.20a-b) and Fig. 19.1.6c. The sum of $\delta^-/2$ and $\delta^+/2$ is the total splitting Ω^R , their difference is the detuning Δ, and the shift product $\delta^-\delta^+$ is the Rabi rate squared.

$$\delta^-/2+\delta^+/2=\Omega^R\quad(19.1.20f)\qquad \delta^-/2-\delta^+/2=\Delta\quad(19.1.20g)\qquad .\delta^-\delta^+=r^2\quad(19.1.20h)$$

Finally, note the AC Stark state norm.

$$\delta^\pm+r^2=(\Omega^R\pm\Delta)^2+r^2=2\Omega^R(\Omega^R\pm\Delta)=2\Omega^R\delta^\pm \qquad (19.1.20i)$$

The AC Stark states are also called *adiabatic dressed eigenstates* because the dipole moment $\mathbf{p}_\perp$ or $\mathbf{m}_\perp$ oscillation is correlated or "clothed" with that of the stimulating radiation particularly near resonance. They are the states that arise from a zero-field eigenstate if r or Δ are turned on slowly (adiabatic).

Consider two AC dressed eigenstate amplitudes in a 50-50 duet at frequencies Ω^{hi} and Ω^{lo}.

$$e^{-i\Omega^{hi}t}+e^{-i\Omega^{lo}t}=e^{-i(\varepsilon+\delta/2)t}+e^{-i(\omega-\delta/2)t}=e^{-i(\varepsilon+\omega)t/2}\cos(\varepsilon-\omega+\delta)t/2$$

$$=e^{-i\Omega 0t}\cos\Omega^R t/2$$

It is an *amplitude modulation (AM)* of a carrier frequency $\Omega_0=(\varepsilon+\omega)t/2$ by a modulation frequency $\Omega^R t/2$ giving two *side bands* belonging to the two Ω^{hi} and Ω^{lo} curves in Fig. 19.1.6 above and below Ω_0 .

$$\omega_{high\ sideband}=\Omega_0+\Omega^R/2=\Omega^{hi}=\varepsilon+\delta^-/2 \qquad (19.1.18a)$$

$$\omega_{low\ sideband}=\Omega_0-\Omega^R/2=\Omega^{lo}=\omega-\delta^-/2 \qquad (19.1.18b)$$

The modulation arises because the radiating dipole $\mathbf{p}_\perp=p\sin\vartheta^R$ varies with polar angle ϑ^R of spin vector **S** as the crank vector $\mathbf{\Omega}^R$ turns in Fig. 19.1.3. As the **S** vector rotates from the spin-up ground state ($\vartheta^R=0$) the radiation moment beats up and down. For $\Delta=r$, a maximum $\mathbf{p}_\perp=p$ occurs at $\vartheta^R=\pi/2$ as in Fig. 19.1.3b. For $\Delta\sim 0$, angle ϑ^R rotates at uniform rate $\Omega^R\sim r$ from 0 to 2π as in Fig. 19.1.3c. Dipole $\mathbf{p}_\perp$ has beat maxima

at $\pi/2$ and $3\pi/2$ and a zero in between at angle $\vartheta^R=\pi$ of the excited (spin-down) state. As in the discussion of (18.210), amplitude beat frequency is $\Omega^R/2$ while intensity (square-amplitude) beats at Ω^R.

A geometric sketch of the spin-crank angle ϑ^R and related frequencies Ω^R, $\delta^{\pm}$ and Δ is given in Fig. 19.1.7. Concentric circles of radii δ^- and δ^+ define the $\mathbf{\Omega}^R$ vector by (19.1.20f) and Δ by (19.1.20g). The figure relates angles ϑ^R , $\vartheta^R/2$, and components $(\cos\vartheta^R/2, \sin\vartheta^R/2)$ of AC states (19.1.20c-d).

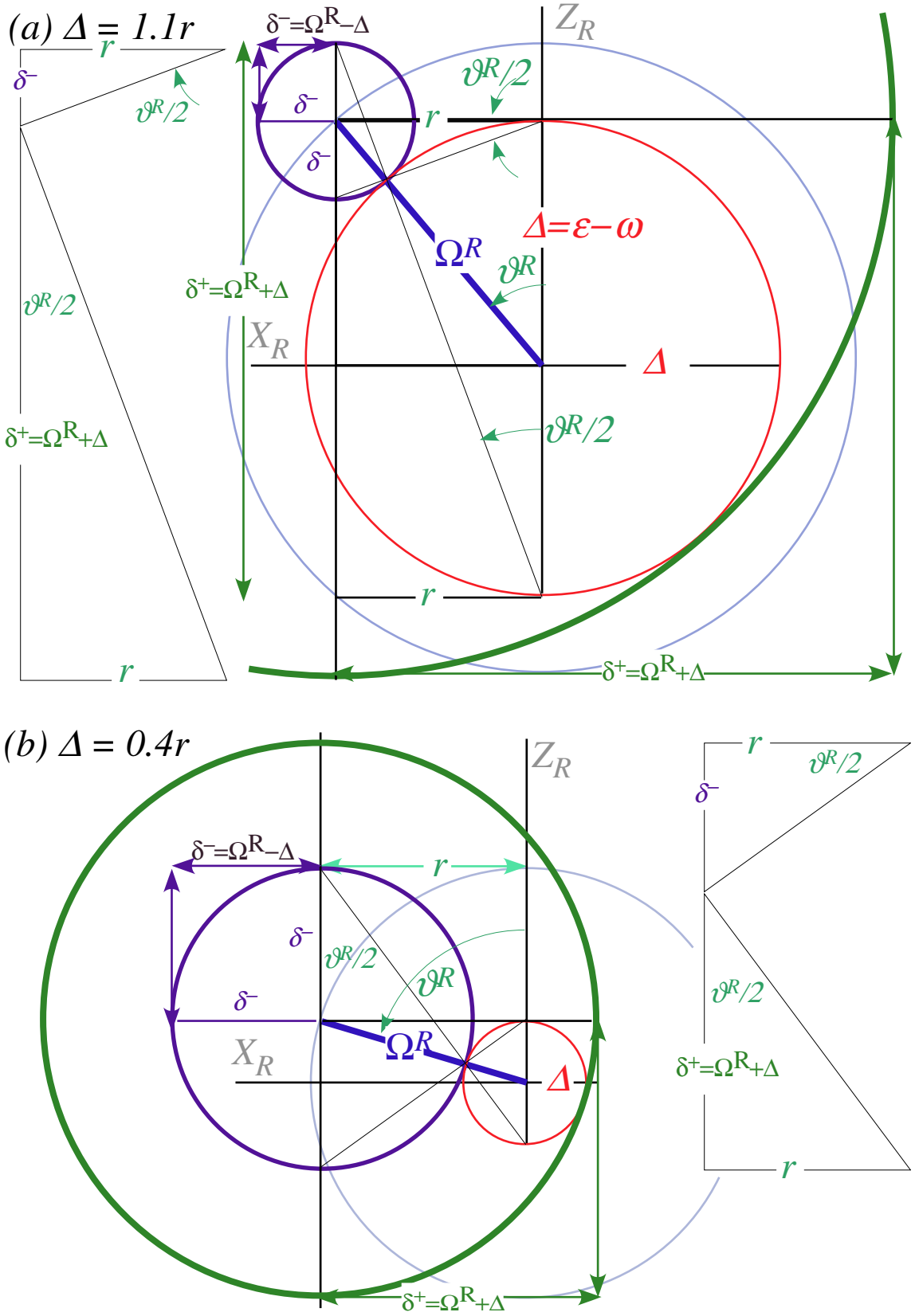

Fig. 19.1.6 AC Stark eigensolution geometry. Rabi rate r=(a) 1.2, (b) 0.4.

Problems for Chapter 19.

Jailhouse Rock'round the Clock(again)

19.1.1 In Problem 18.3.1 (*Jailhouse Rock'n Roll*) prisoner-*M* is in the infinite-well maximum-security prison of Chapter 12 suffering from an Earthquake (caused perhaps by a heavy-metal rock band) that seems to go on forever. *M* remains in any of its eigenstates only in the absence of perturbations. But now the prison floor tilt angle varies: $\phi=\phi^{limit} sin(\omega_{rock}t)$ giving $V_{rock'n\ roll}(x)$ of Problem 18.1.1. Using only the first term in $V_{rock'n\ roll}(x)$, discuss transition from the ground state $|\varepsilon_1\rangle$ to $|\varepsilon_2\rangle$ stimulated by frequency ω_{rock} of amplitude $\phi^{limit}=\pi/10$. At first assume no other levels participate, then estimate possible "leakage.".

(a) $\omega_{rock} = \varepsilon_1$ (*=1* in theorist $\hbar=1$ units)

(b) $\omega_{rock} = 2\varepsilon_1$.

(c) $\omega_{rock} = 3\varepsilon_1$..

(d) $\omega_{rock} = 4\varepsilon_1$...

In each case plot the resulting Rabi-Spin **S**-vector and its driving crank **Ω**-vector. Indicate on a plot like Fig. 19.1.6 the dressed eigenstates and the maximum transition amplitude.